Research in Astronomy and Astrophysics, 25:035005 (7pp), 2025 March

https://doi.org/10.1088/1674-4527/adb55a
CSTR: 32081.14.RAA.adb55a

Kilonova Emission from Neutron Star Mergers with Different Equations of State

Wu-Zimo Qiumu[1], Meng-Hua Chen[2], Qiu-Hong Chen[1], and En-Wei Liang[1]
[1] Guangxi Key Laboratory for Relativistic Astrophysics, School of Physical Science and Technology, Guangxi University, Nanning 530004, China; lew@gxu.edu.cn
[2] Kavli Institute for Astronomy and Astrophysics, Peking University, Beijing 100871, China; physcmh@pku.edu.cn
Received 2024 August 28; revised 2025 January 16; accepted 2025 January 29; published 2025 March 4

Abstract

A kilonova is an optical-infrared transient powered by the radioactive decay of heavy nuclei from a binary neutron star merger. Its observational characteristics depend on the mass and the nuclide composition of merger ejecta, which are sensitive to the equation of state (EoS) of the neutron star. We use astrophysical conditions derived from different EoSs as nucleosynthesis inputs to explore the impact of various EoS on the *r*-process nucleosynthesis and the kilonova emission. Our results show that both the abundance patterns of merger ejecta and kilonova light curves are strongly dependent on the neutron star EoSs. Given the mass of two neutron stars, the merger with a softer EoS tends to generate a larger amount of ejected material, and may lead to a brighter kilonova peak luminosity. The relationship between the neutron star EoS and the peak luminosity provides a probe for constraining the properties of EoS in multi-messenger observations of neutron star mergers.

Key words: nuclear reactions, nucleosynthesis, abundances – equation of state – stars: neutron

1. Introduction

It has long been considered that mergers of neutron stars or neutron star-black hole systems are promising astrophysical sites for the production of heavy elements beyond iron through the rapid neutron capture process (*r*-process, Burbidge et al. 1957; Lattimer & Schramm 1974). The radioactive decay of heavy *r*-process nuclei from merger ejecta powers an optical-infrared transient known as a kilonova (Li & Paczyński 1998; Metzger et al. 2010; Korobkin et al. 2012; Barnes & Kasen 2013; Kasen et al. 2013; Barnes et al. 2016; Metzger 2019). In 2017, the LIGO/Virgo collaboration discovered the first gravitational wave signal generated by a binary neutron star merger (GW170817), with individual masses ranging from 1.17 to 1.60$M_\odot$ and a total mass of $2.74^{+0.04}_{-0.01}M_\odot$ (Abbott et al. 2017a). However, without the spin restriction, the masses of neutron stars would range between 0.86 and 2.26$M_\odot$ (Abbott et al. 2017a). Subsequently, this gravitational wave event was found to be followed by a gamma-ray burst (GRB 170817A. Goldstein et al. 2017) and a kilonova (AT2017gfo, Abbott et al. 2017b; Arcavi et al. 2017; Coulter et al. 2017; Cowperthwaite et al. 2017; Drout et al. 2017; Evans et al. 2017; Kasen et al. 2017; Kasliwal et al. 2017; Pian et al. 2017; Shappee et al. 2017; Smartt et al. 2017). The features of the kilonova AT2017gfo are in good agreement with predictions of *r*-process kilonova models (Cowperthwaite et al. 2017; Drout et al. 2017; Evans et al. 2017; Kasliwal et al. 2017; Nicholl et al. 2017; Pian et al. 2017; Smartt et al. 2017; Tanvir et al. 2017), suggesting the synthesis of $\sim$0.05$M_\odot$ of heavy *r*-process nuclei in the ejected material. Watson et al. (2019) analyzed the absorption features in the observed kilonova spectra and identified strontium, a heavy element with atomic number $Z = 38$, in the merger ejecta. These observational evidences indicate that the mergers of two neutron stars are the primary sources of heavy *r*-process nuclei (Kasen et al. 2017; Hotokezaka et al. 2018; Chen et al. 2024a).

Observations of kilonova transients provide unique insight into the mass ejection from mergers and the nuclear composition of merger ejecta (Kasen et al. 2017; Watson et al. 2019; Wu et al. 2019; Domoto et al. 2021, 2022; Hotokezaka et al. 2023; Chen & Liang 2024; Levan et al. 2024). However, estimating the mass of the ejected material involves many systematic uncertainties, including astrophysical conditions (see Shibata & Hotokezaka 2019; Radice et al. 2020 for reviews) and nuclear physics inputs (see Mumpower et al. 2016; Cowan et al. 2021 for reviews). In nuclear physics, properties of *r*-process nuclei, such as nuclear masses, β-decay half-lives, neutron capture rates, and fission distributions, remain unmeasured. Consequently, it remains a challenge to accurately describe the nuclear heating rate generated by the radioactive decay of *r*-process nuclei. Zhu et al. (2021) proposed that uncertainties in nuclear physics often lead to at least one order of magnitude variation in the inferred mass of ejected material from kilonova light curves. In astrophysics, simulations of neutron star mergers require consideration of extremely strong gravitational and magnetic fields, as well as densities and temperatures that exceed those observed in many other astrophysical phenomena. Radice et al. (2018) revealed that the amount and properties of the ejected material from neutron star mergers are highly sensitive to both binary parameters and the neutron star equation of state (EoS). On the one hand, the fate of the merger remnant is significantly

dependent on the EoS, which determines the allowed maximum mass for neutron stars (Özel & Freire 2016). The central merger remnant with masses exceeding the maximum mass can collapse into black holes. Conversely, if the mass of a post-merger remnant is less than the allowed maximum mass, it may be from either a massive neutron star or a stable neutron star. This has significant implications, as the central neutron star remnant can shed mass into an accretion disk, eject material via disk winds, and serve as a strong source of neutrinos, which can alter the electron fraction. On the other hand, the mass of ejected material in the presence of a neutron star remnant is also highly dependent on the EoS (Bauswein et al. 2013; Hotokezaka et al. 2013; Sekiguchi et al. 2016; Radice et al. 2018; Rosswog & Korobkin 2024). For example, a stiff EoS results in neutron stars of a given mass having larger radii compared to those with a soft EoS. This leads to more pronounced tidal effects, causing earlier mergers at higher orbital separations and lower orbital velocities. Additionally, stiff EoSs have higher sound speeds, making it more difficult to shock neutron star matter. Due to the less efficient shock heating and less violent post-merger oscillations, the mass ejection from neutron star mergers is significantly affected. Therefore, it is worthwhile to consider the impact of neutron star EoS on kilonova emission, as it may provide a probe for the EoS through kilonova light curves.

The relation between kilonova luminosity and neutron star EoS was investigated by Zhao et al. (2023). Without using *r*-process nucleosynthesis simulations, they adopted a semi-analytical model to calculate kilonova light curves under different EoSs and found that peak luminosities are sensitive to neutron star EoS. However, their research neglected the impact of EoS on *r*-process nucleosynthesis, including the detailed evolution process of heavy elements, nuclear heating rates, and radiative transfer processes. In this paper, we focus on exploring the impact of EoS on the nuclear composition of merger ejecta and the resulting kilonova light curve through detailed *r*-process simulations for binary neutron star mergers. By using numerical relativistic simulation results as astrophysical input for the *r*-process network, as well as detailed modeling for kilonova radiation produced by the radioactive decay of heavy *r*-process nuclei, we aim to further investigate the relationship between kilonova luminosity and EoS.

This paper is organized as follows. Section 2 details the *r*-process nucleosynthesis and the procedure to calculate the kilonova emission. Section 3 presents the kilonova emission results obtained using various neutron star EoSs. Conclusions and discussions are provided in Section 4.

2. Methods

2.1. r-Process Nucleosynthesis

To obtain the detailed composition of heavy *r*-process nuclei, we use the improved version of the nuclear reaction network SkyNet (Lippuner & Roberts 2015, 2017) to perform *r*-process nucleosynthesis simulations. The nuclear physics data and the nuclear reaction rates are the same as in our previous work (Chen et al. 2023, 2024b, 2025). For the radioactive decay energy data of heavy *r*-process nuclei, we use the recent database from the Evaluated Nuclear Data File library (ENDF/B-VIII.0, Brown et al. 2018). The astrophysical inputs for different EoSs are taken from the numerical relativity simulations provided by Radice et al. (2018).

Following Chen & Liang (2024), the total *r*-process heating rate is given by

$$\dot{Q}(t) = f(t)\dot{q}(t), \tag{1}$$

where $f(t)$ and $\dot{q}(t)$ represent the thermalization efficiency and radioactive energy generation rate, respectively. The radioactive decay energy released by heavy *r*-process nuclei in the merger ejecta can be written as

$$\dot{q}(t) = N_{\rm A}\sum_i \lambda_i E_i Y_i(t), \tag{2}$$

where λ_i is the nuclear reaction rate of the ith nucleus, E_i is the radioactive decay energy, $Y_i(t)$ is the elemental abundance, and $N_{\rm A}$ is Avogadro's number. The thermalization efficiency follows the analytic formula provided by Barnes et al. (2016)

$$f(t) = 0.36\left[\exp(-0.56t_{\rm day}) + \frac{\ln(1+0.34t_{\rm day}^{0.74})}{0.34t_{\rm day}^{0.74}}\right], \tag{3}$$

where $t_{\rm day}$ is the time in days after the merger.

For the electron fraction $Y_{\rm e}$, we adopt the analytical formula fitted by Nedora et al. (2022)

$$Y_{\rm e}(q,\tilde{\Lambda}) = b_0 + b_1 q + b_2\tilde{\Lambda} + b_3 q^2 + b_4 q\tilde{\Lambda} + b_5\tilde{\Lambda}^2, \tag{4}$$

where q is the mass ratio of binary neutron stars, $\tilde{\Lambda}$ is the reduced tidal deformability parameter (Nedora et al. 2022), and b_0 to b_5 are fitting coefficients. We use the best-fit parameters provided by Nedora et al. (2022). The opacity κ as a function of $Y_{\rm e}$ is based on the results provided by Tanaka et al. (2020), which were derived from a systematic analysis of the composition of heavy elements.

2.2. Kilonova Model

The kilonova model is based on the work of Chen & Liang (2024). We divide the ejected material into n layers and the density profile can be written as (Chen et al. 2021, 2022)

$$\rho(v_n, t) = \rho_0(t)\left(\frac{v_n}{v_0}\right)^{-3}, \tag{5}$$

where v_n is the expansion velocity of the nth layer. The thermal energy of the merger ejecta evolves according to

$$\frac{dE_n}{dt} = -\frac{E_n}{R_n}\frac{dR_n}{dt} - L_n + \dot{Q}(t)m_n, \tag{6}$$

where R_n is the radius of the nth layer, m_n is the mass of the nth layer, E_n is the internal energy, and L_n is the radiation

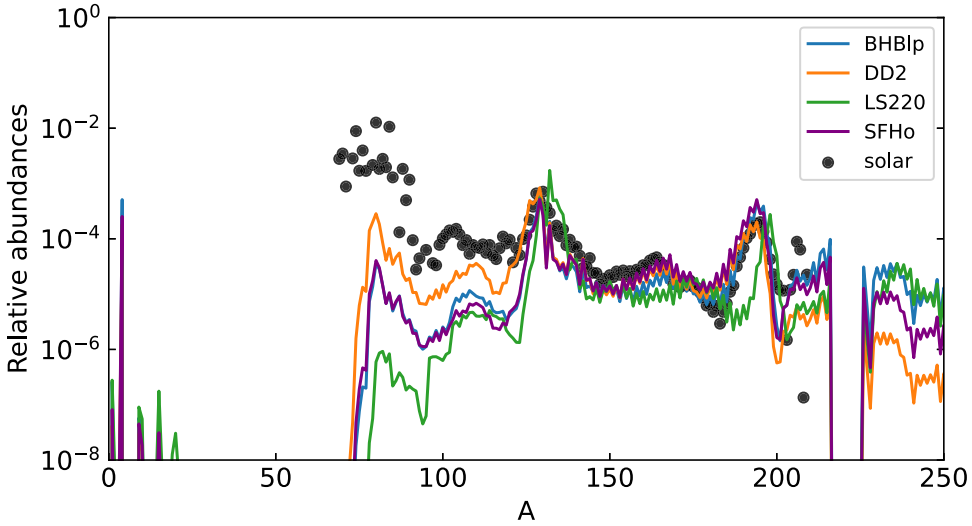

Figure 1. Abundance patterns of *r*-process nucleosynthesis calculated using different EoSs. The abundances of solar *r*-process elements taken from Arnould et al. (2007) are also shown for comparison. Astrophysical inputs for different EoSs are adopted from numerical relativity simulations provided by Radice et al. (2018).

luminosity. The thermal luminosity of the nth layer is given by

$$L_n = \frac{E_n}{t_{\mathrm{lc},n} + t_{\mathrm{d},n}}, \tag{7}$$

where $t_{\mathrm{lc},n} = v_n t/c$ is the light-crossing time and $t_{\mathrm{d},n} = \tau_n v_n t/c$ is the photon diffusion timescale, with τ_n being the optical depth. The total kilonova luminosity from all layers can be written as

$$L_{\mathrm{bol}} = \sum_n L_n. \tag{8}$$

3. Results

In Figure 1, we show the resulting abundance patterns derived from *r*-process nucleosynthesis simulations for binary neutron star mergers. The astrophysical inputs for different EoSs, including BHBlp, DD2, LS220, and SFHo, are taken from numerical relativity simulations given by Radice et al. (2018). It can be seen that there are differences in abundance patterns calculated using different EoSs, especially in regions with atomic mass numbers $A \geqslant 200$ and $A \leqslant 120$. This result indicates that the EoS of a neutron star plays a significant role in the *r*-process nucleosynthesis, potentially impacting the light curve of kilonova emission.

Figure 2 shows the kilonova light curves produced by the radioactive decay of heavy *r*-process nuclei. Here we use the wide-band filters of the Near Infrared Camera (NIRCam) on the JWST.[3] The characteristic radii ($R_{1.35}$) of a non-rotating neutron star with a mass of $1.35M_\odot$ calculated using the EoS from SFHo, LS220, BHBlp, and DD2 are 11.92, 12.64, 13.21 and 13.21 km, respectively. The BHBlp and DD2 predict the same radii for neutron star masses up to $1.5M_\odot$, but DD2 predicts a larger radius than BHBlp for masses above $1.5M_\odot$. Generally, an EoS with a smaller $R_{1.35}$ is regarded as "softer," whereas an EoS with a larger $R_{1.35}$ is deemed "stiffer." Therefore, among these selected EoSs, SFHo is the softest and DD2 is the stiffest. As can be seen in Figure 2, a softer EoS leads to brighter kilonova light curves and higher peak luminosity. For example, in the band of F200W, the peak luminosity calculated with soft EoS, SFHo, is higher than that calculated with stiff EoS, DD2, by a factor of $\sim$2.4 while that in the band of F444W is $\sim$3.7.

To further investigate the relation between neutron star EoS and the peak luminosity, we perform *r*-process nucleosynthesis simulations using 40 distinct EoSs obtained from numerical relativistic simulations provided by Bauswein et al. (2013). In Figure 3, we show the relationship between the electron fraction Y_{e} and the characteristic radius $R_{1.35}$. It is found that softer and stiffer EoSs tend to produce smaller values of Y_{e}. Figure 4 shows the relationship between peak luminosity and characteristic radius $R_{1.35}$ for different EoSs. Solid circles represent simulation results for a symmetric binary system with two neutron star masses of $1.35 + 1.35M_\odot$. It can be observed that as the characteristic radius $R_{1.35}$ decreases, the mass of the merger ejecta increases significantly, leading to a brighter peak luminosity. Our analysis indicates that the kilonova flux calculated using the softest EoS exceeds that calculated with the stiffest EoS by a factor of $\sim$3.13. This can be attributed to the fact that softer EoSs have a smaller characteristic radius $R_{1.35}$, resulting in a reduction of the tidal disruption radius during neutron star mergers. This enhances the efficiency of shock heating and amplifies the kinetic energy of the

[3] https://jwst-docs.stsci.edu/jwst-near-infrared-camera

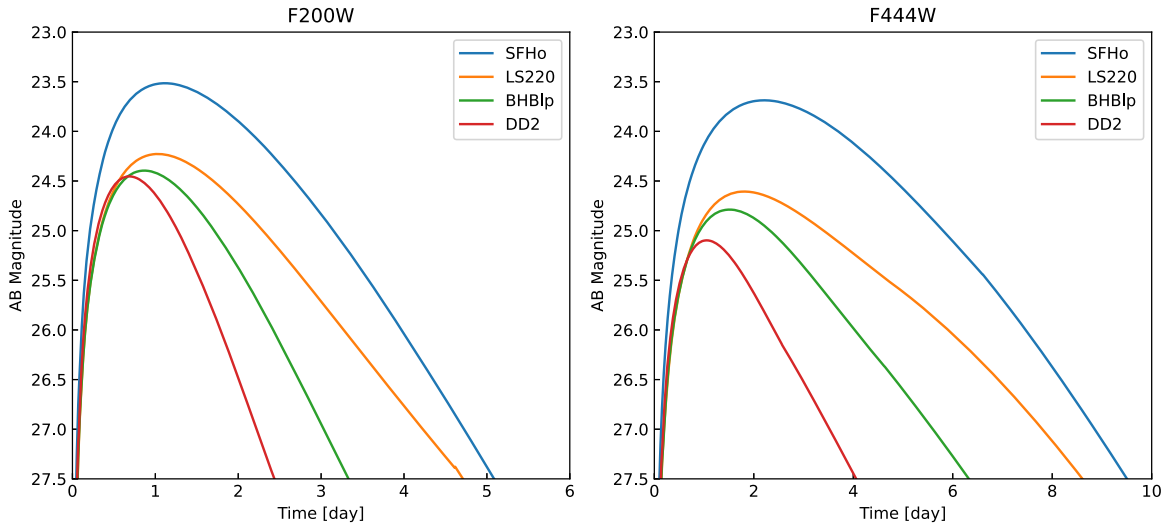

Figure 2. Kilonova light curves in the bands of F200W (left panel) and F444W (right panel) produced by the radioactive decay of *r*-process nuclei for ejecta from the merger of a symmetrical neutron star binary with the mass of $1.35 + 1.35M_{\odot}$. The blue, orange, green, and red lines represent the kilonova light curves calculated using EoS from SFHo, LS220, BHBlp, and DD2, respectively. The distance to the source is set to 200 Mpc.

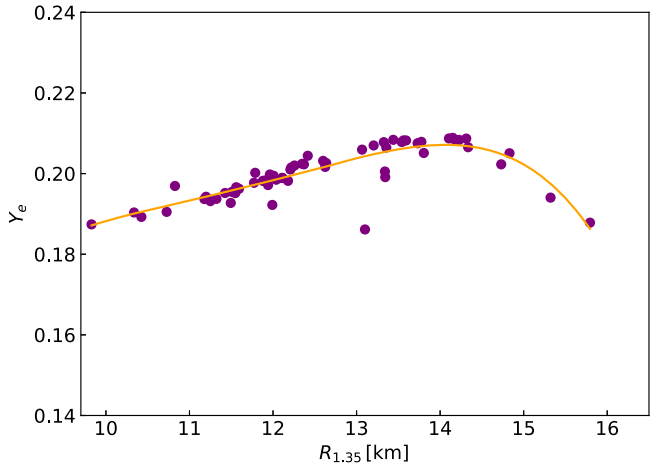

Figure 3. The electron fraction Y_e as a function of the characteristic radius $R_{1.35}$ for different EoSs. Solid circles represent the results for different EoSs obtained using the analytical formula from Nedora et al. (2022). The solid line shows the polynomial fitting result.

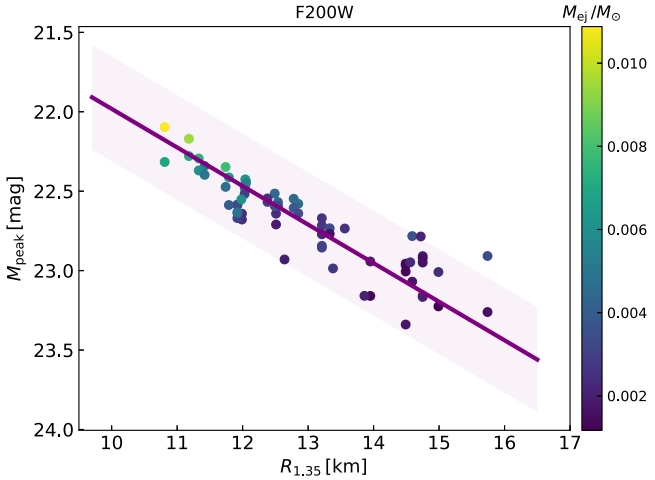

Figure 4. The relation between peak kilonova luminosity and the characteristic radius derived from different EoSs. Solid circles indicate simulation results for a symmetric binary merger with masses of $1.35 + 1.35M_{\odot}$. The solid line represents the linear fitting result, and the colored region indicates the $\pm 1\sigma$ range.

oscillations. Consequently, a larger amount of merger ejecta is generated, leading to brighter kilonova emission. This indicates that, given the mass of the binary neutron star system, the observation of kilonova emission can provide information about the neutron star EoS.

We further investigate the ejected material produced by binary neutron star mergers with different masses. We utilize the analytical fitting result for ejecta mass obtained from numerical relativistic simulations by Radice et al. (2018). Figure 5 shows the mass value of merger ejecta as a function of two neutron star masses obtained using four different EoSs, including SFHo, LS220, DD2, and BHBlp. It is found that in a symmetric binary system, larger neutron star masses lead to more ejected material. The neutron star EoS with softer properties such as SFHo and LS220 tends to generate a greater amount of merger ejecta compared to BHBlp and DD2. This result is consistent with the numerical relativistic simulation conducted by Kasen et al. (2013) and Tanaka & Hotokezaka (2013). Based on the ejected material from two neutron star mergers with different masses, we calculate the peak luminosity of their kilonova emission, as shown in Figure 6.

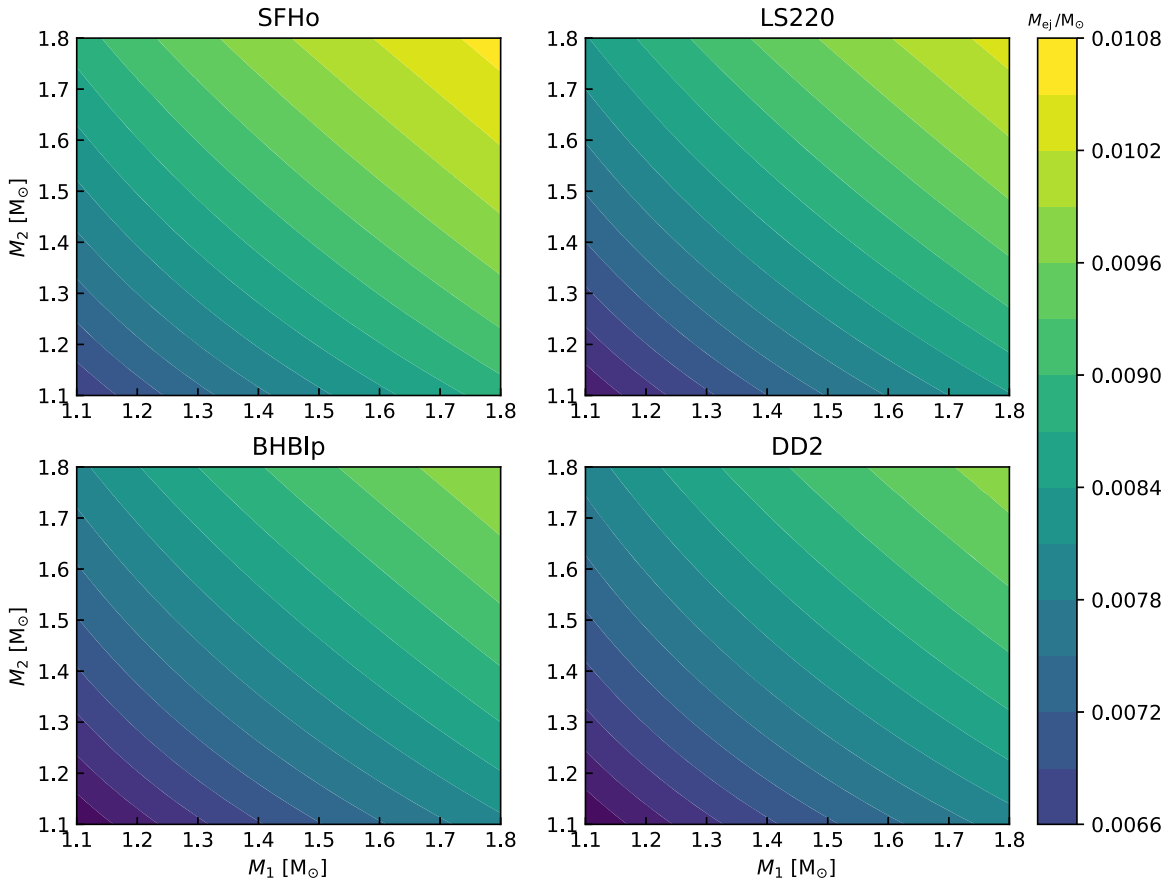

Figure 5. The mass value of merger ejecta as a function of two neutron star masses. Here we use the analytical fitting result for ejecta mass obtained from numerical relativistic simulations by Radice et al. (2018).

It is found that the peak brightness of a kilonova increases as the binary mass increases. Notably, it can be seen that within the same binary neutron star system, a softer EoS leads to a brighter kilonova. This result suggests that kilonova emission provides a direct probe for constraining the neutron star EoS.

4. Conclusions and Discussions

In this work, we considered the neutron star EoS in binary neutron star mergers and explored its impact on the *r*-process nucleosynthesis and kilonova emission. Through detailed *r*-process nucleosynthesis simulations, we investigated the impact of the neutron star EoS on the abundance patterns of *r*-process elements. It was observed that there are differences in abundance patterns calculated using different EoSs, particularly in regions with atomic mass numbers $A \geqslant 200$ and $A \leqslant 120$ (Figure 1). This result suggests that the neutron star EoS plays a significant role in *r*-process simulations, potentially affecting the light curve of kilonova emission.

According to the detailed composition obtained from *r*-process simulations, we calculated kilonova light curves powered by the radioactive decay of heavy nuclei (Figure 2). It is found that the peak luminosity calculated with a soft EoS is higher than that calculated with a stiff EoS. To further investigate the relation between neutron star EoS and the peak luminosity, we performed *r*-process nucleosynthesis simulations using 40 distinct EoSs obtained from numerical relativistic simulations. It can be observed that kilonova emission is directly related to the neutron star EoS: a softer EoS leads to brighter kilonova light curves and higher peak luminosity (Figure 4). This result is consistent with that obtained using the simple analytical formula adopted in Bauswein et al. (2013). This can be attributed to the fact that softer EoSs have a smaller characteristic radius $R_{1.35}$, resulting in a reduction of the tidal disruption radius during neutron star mergers. This enhances the efficiency of shock heating and amplifies the kinetic energy of the oscillations. Consequently, a larger amount of merger ejecta is generated, leading to brighter kilonova emission. These results are consistent with previous results (Bauswein et al. 2013; Hotokezaka et al. 2013; Sekiguchi et al. 2016; Radice et al. 2018; Rosswog & Korobkin 2024). We further investigate the ejected material

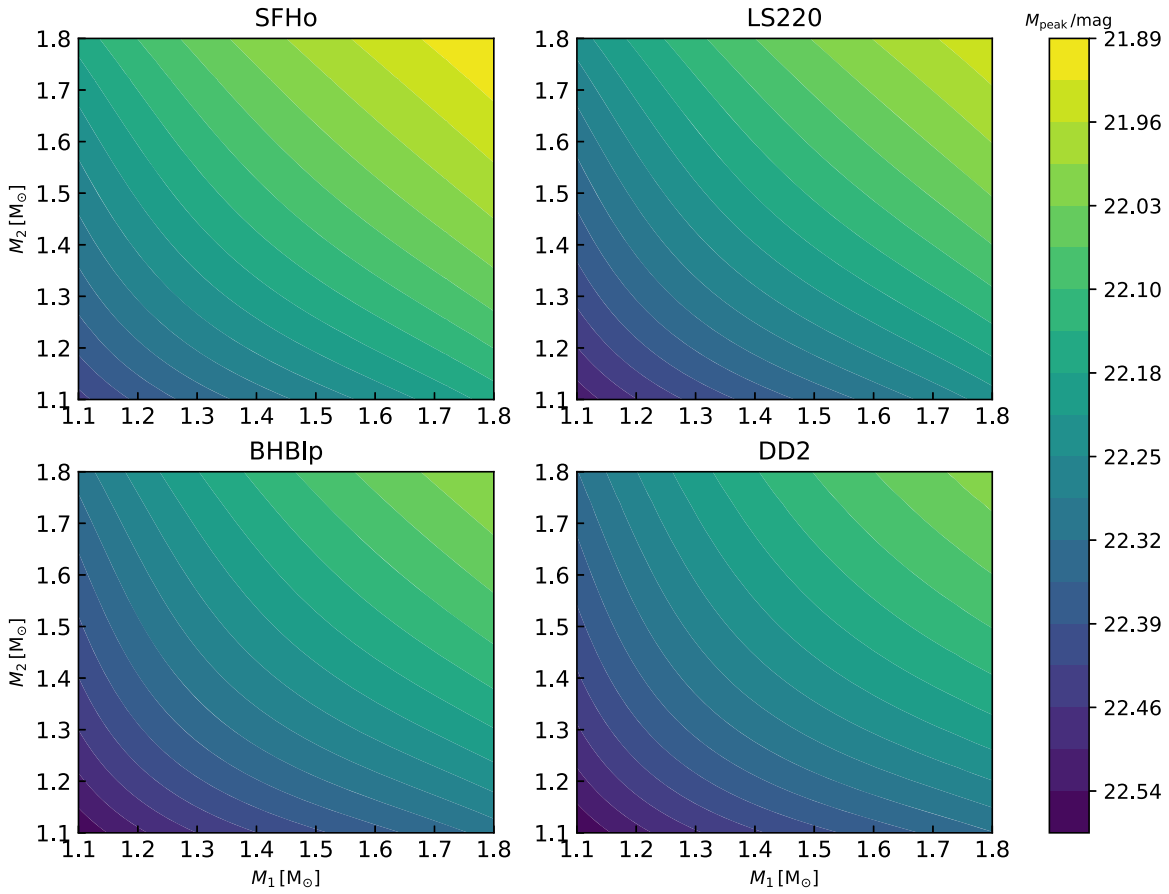

Figure 6. The same as Figure 5, but for the peak luminosity in the near-infrared band.

produced by binary neutron star mergers with different masses (Figures 5 and 6). The neutron star EoS with softer properties such as SFHo and LS220 tend to generate a greater amount of merger ejecta and power a brighter kilonova emission compared to BHBlp and DD2. This result suggests that kilonova emission provides a direct probe for constraining the neutron star EoS.

It is worth noting that our astrophysical conditions for the *r*-process nucleosynthesis calculations are obtained from numerical relativistic simulations, which typically produce merger ejecta with mass lower than those inferred from the observed kilonova light curves by about one order of magnitude (Siegel 2019). This could be due to the uncertainty in nuclear physics inputs, as the properties of heavy *r*-process nuclei are often unmeasured (Barnes et al. 2021; Zhu et al. 2021; Chen et al. 2025). Zhu et al. (2021) show that uncertainties from nuclear physics can lead to at least one order of magnitude uncertainty in kilonova luminosity. It should be noted that nuclear physics uncertainties do not affect our main conclusions, as nuclear properties are intrinsic characteristics that will influence the behavior of all kilonovae.

Multi-messenger observations of the first neutron star merger event GW170817/GRB 170817A/AT2017gfo (Abbott et al. 2017b) provide a solid case for studying the neutron star EoS. The peak luminosity of kilonova AT2017gfo appears brighter than our calculated results (with a distance of 40 Mpc), suggesting that the observed light curves support a soft EoS (i.e., smaller characteristic radius for a given mass neutron star). This is consistent with those results derived from the analysis of tidal deformability from GW170817 which suggest that the neutron star radius must be $\lesssim$13 km (Abbott et al. 2018; De et al. 2018; Raithel et al. 2018). Note that we adopted a spherically symmetric model in kilonova calculations, which may affect the kilonova peak luminosity (Zhu et al. 2020; Korobkin et al. 2021). However, recent analysis has shown that the merger ejecta of the kilonova AT2017gfo is highly spherical, and the distribution of heavy elements is uniform (Sneppen et al. 2023).

In order to effectively utilize the direct relationship between the kilonova peak luminosity and the neutron star EoS to study the properties of dense nuclear matter, the masses of two neutron stars need to be specified. The determination of neutron

star masses typically depends on observations from gravitational wave observatories such as LIGO/Virgo. Given the success of the joint detection of GW170817 and AT2017gfo, there is great potential for probing the neutron star EoS based on multi-messenger analysis in the future. However, due to the degeneracy of multiple parameters, there is still some uncertainty in the neutron star masses obtained from gravitational wave signals. As the LIGO/Virgo detectors improve, the constraints on neutron star masses will be greatly enhanced. The ongoing LIGO/Virgo O4 run is expected to detect gravitational wave sources from neutron star mergers within a distance of 200 Mpc and may detect ∼10 merger events. Additionally, the JWST is a powerful infrared instrument for observing kilonovae, offering a comprehensive view of kilonova emission from early to late phases (Chen & Liang 2024).

Acknowledgments

We thank Li-Xin Li for the valuable discussion. This work is supported by the National Natural Science Foundation of China (NSFC, grant Nos. 12403043, 12347172, and 12133003). M.H.C. also acknowledges support from the China Postdoctoral Science Foundation (grant Nos. GZB20230029 and 2024M750057). This work is also supported by the Guangxi Talent Program (Highland of Innovation Talents).

ORCID iDs

Meng-Hua Chen https://orcid.org/0000-0001-8406-8683
Qiu-Hong Chen https://orcid.org/0009-0006-8625-5283
En-Wei Liang https://orcid.org/0000-0002-7044-733X

References

Abbott, B. P., Abbott, R., Abbott, T. D., et al. 2017a, PhRvL, 119, 161101
Abbott, B. P., Abbott, R., Abbott, T. D., et al. 2017b, ApJL, 848, L12
Abbott, B. P., Abbott, R., Abbott, T. D., et al. 2018, PhRvL, 161101, 121
Arcavi, I., Hosseinzadeh, G., Howell, D. A., et al. 2017, Natur, 551, 64
Arnould, M., Goriely, S., & Takahashi, K. 2007, PhR, 450, 97
Barnes, J., & Kasen, D. 2013, ApJ, 775, 18
Barnes, J., Kasen, D., Wu, M.-R., & Martínez-Pinedo, G. 2016, ApJ, 829, 110
Barnes, J., Zhu, Y. L., Lund, K. A., et al. 2021, ApJ, 918, 44
Bauswein, A., Goriely, S., & Janka, H. T. 2013, ApJ, 773, 78
Brown, D. A., Chadwick, M. B., Capote, R., et al. 2018, NDS, 148, 1
Burbidge, E. M., Burbidge, G. R., Fowler, W. A., & Hoyle, F. 1957, RvMP, 29, 547
Chen, M.-H., Hu, R.-C., & Liang, E.-W. 2022, ApJL, 932, L7
Chen, M.-H., Hu, R.-C., & Liang, E.-W. 2023, MNRAS, 520, 2806
Chen, M.-H., Li, L.-X., Chen, Q.-H., Hu, R.-C., & Liang, E.-W. 2024a, MNRAS, 529, 1154
Chen, M.-H., Li, L.-X., & Liang, E.-W. 2024b, ApJ, 971, 143
Chen, M.-H., Li, L.-X., Liang, E.-W., & Wang, N. 2025, A&A, 693, A1
Chen, M.-H., Li, L.-X., Lin, D.-B., & Liang, E.-W. 2021, ApJ, 919, 59
Chen, M.-H., & Liang, E.-W. 2024, MNRAS, 527, 5540
Coulter, D. A., Foley, R. J., Kilpatrick, C. D., et al. 2017, Sci, 358, 1556
Cowan, J. J., Sneden, C., Lawler, J. E., et al. 2021, RvMP, 93, 015002
Cowperthwaite, P. S., Berger, E., Villar, V. A., et al. 2017, ApJL, 848, L17
De, S., Finstad, D., Lattimer, J. M., et al. 2018, PhRvL, 121, 091102
Domoto, N., Tanaka, M., Kato, D., et al. 2022, ApJ, 939, 8
Domoto, N., Tanaka, M., Wanajo, S., & Kawaguchi, K. 2021, ApJ, 913, 26
Drout, M. R., Piro, A. L., Shappee, B. J., et al. 2017, Sci, 358, 1570
Evans, P. A., Cenko, S. B., Kennea, J. A., et al. 2017, Sci, 358, 1565
Goldstein, A., Veres, P., Burns, E., et al. 2017, ApJL, 848, L14
Hotokezaka, K., Beniamini, P., & Piran, T. 2018, IJMPD, 27, 1842005
Hotokezaka, K., Kiuchi, K., Kyutoku, K., et al. 2013, PhRvD, 87, 024001
Hotokezaka, K., Tanaka, M., Kato, D., & Gaigalas, G. 2023, MNRAS, 526, L155
Kasen, D., Badnell, N. R., & Barnes, J. 2013, ApJ, 774, 25
Kasen, D., Metzger, B., Barnes, J., Quataert, E., & Ramirez-Ruiz, E. 2017, Natur, 551, 80
Kasliwal, M. M., Nakar, E., Singer, L. P., et al. 2017, Sci, 358, 1559
Korobkin, O., Rosswog, S., Arcones, A., & Winteler, C. 2012, MNRAS, 426, 1940
Korobkin, O., Wollaeger, R. T., Fryer, C. L., et al. 2021, ApJ, 910, 116
Lattimer, J. M., & Schramm, D. N. 1974, ApJL, 192, L145
Levan, A. J., Gompertz, B. P., Salafia, O. S., et al. 2024, Natur, 626, 737
Li, L.-X., & Paczyński, B. 1998, ApJL, 507, L59
Lippuner, J., & Roberts, L. F. 2015, ApJ, 815, 82
Lippuner, J., & Roberts, L. F. 2017, ApJS, 233, 18
Metzger, B. D. 2019, LRR, 23, 1
Metzger, B. D., Martínez-Pinedo, G., Darbha, S., et al. 2010, MNRAS, 406, 2650
Mumpower, M. R., Surman, R., McLaughlin, G. C., & Aprahamian, A. 2016, PrPNP, 86, 86
Nedora, V., Schianchi, F., Bernuzzi, S., et al. 2022, CQGra, 39, 015008
Nicholl, M., Berger, E., Kasen, D., et al. 2017, ApJL, 848, L18
Özel, F., & Freire, P. 2016, ARA&A, 54, 401
Pian, E., D'Avanzo, P., Benetti, S., et al. 2017, Natur, 551, 67
Radice, D., Bernuzzi, S., & Perego, A. 2020, ARNPS, 70, 95
Radice, D., Perego, A., Hotokezaka, K., et al. 2018, ApJ, 869, 130
Raithel, C. A., Özel, F., & Psaltis, D. 2018, ApJL, 857, L23
Rosswog, S., & Korobkin, O. 2024, AnP, 536, 2200306
Sekiguchi, Y., Kiuchi, K., Kyutoku, K., Shibata, M., & Taniguchi, K. 2016, PhRvD, 93, 124046
Shappee, B. J., Simon, J. D., Drout, M. R., et al. 2017, Sci, 358, 1574
Shibata, M., & Hotokezaka, K. 2019, ARNPS, 69, 41
Siegel, D. M. 2019, EPJA, 55, 203
Smartt, S. J., Chen, T. W., Jerkstrand, A., et al. 2017, Natur, 551, 75
Sneppen, A., Watson, D., Bauswein, A., et al. 2023, Natur, 614, 436
Tanaka, M., & Hotokezaka, K. 2013, ApJ, 775, 113
Tanaka, M., Kato, D., Gaigalas, G., & Kawaguchi, K. 2020, MNRAS, 496, 1369
Tanvir, N. R., Levan, A. J., González-Fernández, C., et al. 2017, ApJL, 848, L27
Watson, D., Hansen, C. J., Selsing, J., et al. 2019, Natur, 574, 497
Wu, M.-R., Barnes, J., Martínez-Pinedo, G., & Metzger, B. D. 2019, PhRvL, 122, 062701
Zhao, C., Lu, Y., Chu, Q., & Zhao, W. 2023, MNRAS, 522, 912
Zhu, J.-P., Yang, Y.-P., Liu, L.-D., et al. 2020, ApJ, 897, 20
Zhu, Y. L., Lund, K. A., Barnes, J., et al. 2021, ApJ, 906, 94